A mechanistic study of Lewis acid-catalyzed covalent organic framework formation

ERIC L. SPITLER, MARISSA R. GIOVINO,

SARAH L. WHITE, AND WILLIAM R. DICHTEL*

Department of Chemistry and Chemical Biology, Cornell University,

Baker Laboratory, Ithaca, New York, USA 14853-1301

Electronic Supplementary Information

Correspondence Address

Professor William R Dichtel
Department of Chemistry and Chemical Biology
Cornell University
Baker Laboratory
Ithaca, NY 14853-1301 (USA)
Tel: (+1)-607-254-2356
Fax: (+1)-607-255-4137
Email: wdichtel@cornell.edu

Table of Contents

A. Materials and Methods

All reagents were purchased from commercial sources and used without further purification. CH_2Cl_2, CH_3CN, and MeOH were purchased from commercial sources and purified using a custom-built alumina-column based solvent purification system. Other solvents were purchased from commercial sources and used without further purification. Infrared spectra were recorded on a Thermo Nicolet iS10 with a diamond ATR attachment and are uncorrected. Ultraviolet/visible/near infrared absorbance spectra were recorded on a Varian Cary 5000 spectrophotometer with a Hg lamp in either CH_2Cl_2 solution or as solids using a praying mantis diffuse reflectance accessory. *In situ* infrared spectra were recorded on an Applied Systems Inc. ReactIR 1000 spectrometer fitted with a 30-bounce silicon-tipped probe. The spectra were acquired in 16 scans at a resolution of 4 cm^{-1}, and the absorbance at 1335 cm^{-1} was monitored over the course of the reaction. IR spectra were recorded every 3 s. X-ray diffraction was performed on a Rigaku Smartlab powder x-ray diffractometer in medium resolution 2θ parallel beam/parallel slit alignment mode employing Cu Kα line focused radiation at 40 kV, 44 mA power and equipped with a Ge crystal detector fitted with a 0.5 mm radiation entrance slit. Samples were mounted on zero background sample holders by dropping powders from a wide-blade spatula and then leveling the sample surface with a glass microscope slide. No sample grinding or sieving was performed prior to analysis. Samples were observed using a 0.04º 2θ step scan (Omega = 1.0º) from 2.0 – 34º with an exposure time of 0.4 s per step. No peaks above the baseline were observed for 2θ > 34º and this region was therefore not considered for further analysis. Thermogravimetric analysis from 20-600 °C was carried out on a TA Instruments Q500 Thermogravimetric Analyzer under a N_2 atmosphere using a 10 °C/min ramp without equilibration delay. Matrix assisted laser desorption ionization time-of-flight (MALDI-TOF) mass spectrometry was performed on a Waters MALDI micro MX MALDI-TOF mass spectrometer using positive ionization and a reflectron detector. The samples were prepared by evaporating a saturated analyte/dithranol matrix solution onto a stainless steel sample plate provided by the manufacturer. Surface area measurements were conducted on a Micromeritics ASAP 2020 Accelerated Surface Area and Porosimetry Analyzer using samples (ca. 20 mg) degassed at 180 °C for 12 hours. N_2 isotherms were generated by incremental exposure to

ultra high purity N_2 up to ca. 1 atm over 28 h in a liquid N_2 (77K) bath, and surface parameters were determined using Langmuir, BET and BJH adsorption models included in the instrument software (Micromeritics ASAP 2020 V1.05). NMR spectra were recorded on a Varian 400 MHz spectrometer equipped with a ^{1}H/X Z-PFG probe at ambient temperature with a 20 Hz sample spin rate. X-ray photoelectron spectroscopy was performed on a Surface Science Instruments Model SSX-100 using monochromated Al Kα radiation (1486.6 eV) and a 5 keV Argon ion beam for sample cleaning.

B. Synthetic Procedures.

Scheme S1. Synthesis of hexahydroxytriphenylene tris(acetonide) **4**.

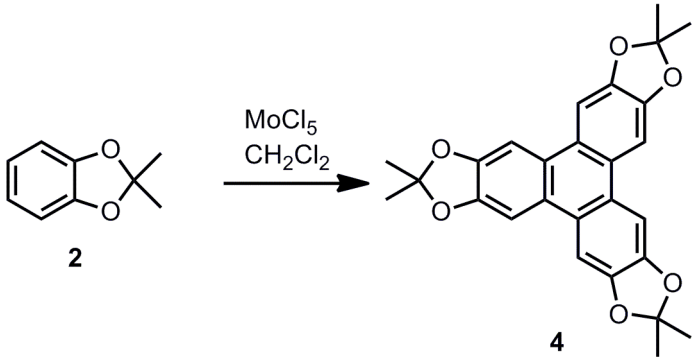

Triphenylene tris(acetonide) 4. Using a modification of a literature procedure,[1] catechol acetonide **2** (0.20 g, 1.34 mmol) was dissolved in anhydrous CH_2Cl_2 (3 mL). $MoCl_5$ (0.37 g, 1.35 mmol) was added to the reaction vessel in three portions (Caution: $MoCl_5$ reacts rapidly with the ambient atmosphere). The resulting black mixture was stirred under N_2 at rt for 20 min, during which time a large amount of gas evolved. The solution was poured into MeOH (10 mL) at 0 °C and was neutralized with a saturated aqueous solution of Na_2CO_3 (50 mL). The dark brown solution was stirred for 10 min and then washed with a 50:50 mixture of EtOAc:hexanes (100 mL), followed by neat EtOAc (3 x 50 mL). The combined organic phases were washed with brine (2 x 50 mL) and water (2 x 50 mL) and evaporated to yield a dark brown oil. The crude product was purified by filtration through a pad of silica gel (4:1 hexanes:EtOAc), followed by evaporation of the solvent to yield **4** as a light brown solid (0.090 g, 45%). **4**: ^{1}H-NMR ($CDCl_3$, 400 MHz) δ 7.68 (s, 6H); 1.77 (s, 18H) ppm. ^{13}C-NMR ($CDCl_3$, 400 MHz) δ 147, 124, 118, 101, 26 ppm. MALDI-MS m/z (%) 443.8 (100, M^+); 444.8 (37, M^++1). IR (powder, ATR) 3083, 2992, 2933,

1493, 1461, 1377, 1292, 1249, 1212, 1159, 985, 968, 842, 784, 756. These spectral data matched those published previously.[2,3]

Scheme S2. Synthesis of Nickel phthalocyanine acetonide **7**.

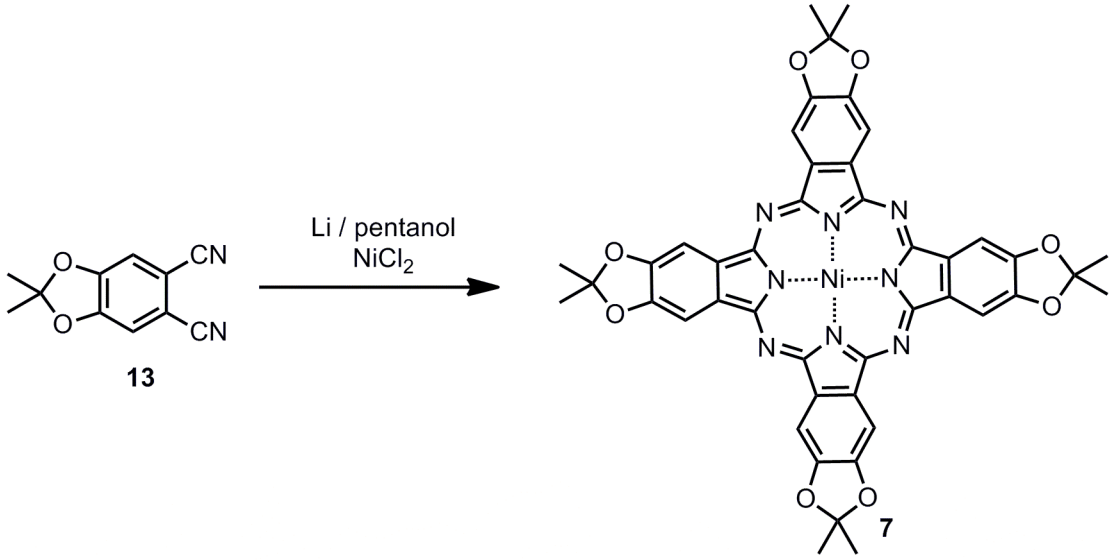

Ni phthalocyanine tetra(acetonide) 7. Phthalonitrile[4] **13** (0.56 g, 2.80 mmol) was dissolved in 1-pentanol (12 mL). Li metal granules (80 mg, 12 mmol) and $NiCl_2$ (360 mg, 2.8 mmol) were added at rt with vigorous stirring. The mixture was heated to reflux (140 $^{\circ}$C) for 5h under a N_2 atmosphere. During this time, the reaction mixture became very dark green. The mixture was cooled to rt, and hexanes (100 mL) was added. A black precipitate formed, which was isolated by centrifugation. This solid was suspended in a minimal amount of $(CH_3)_2CO$ and triturated with H_2O (100 mL). The resulting precipitate was recovered by vacuum filtration and washed with $(CH_3)_2CO$ (20 mL) and CH_2Cl_2 (30 mL) to yield **7** (390 mg, 65%) as a dark blue solid. MALDI-MS m/z (%) 858.2 (100, M^+); 859.2 (66, M^++1); 860.2 (58, M^++2); 861.2 (41, M^++3). IR (powder, ATR) 2989, 2937, 1476, 1426, 1387, 1377, 1351, 1278, 1214, 1099, 1080, 1034, 979, 885, 843, 747. UV-Vis [λ /nm (log ε / M^{-1} cm^{-1}), 1.98 μM in CH_2Cl_2, Fig. S12] 660 (4.74), 635 (4.31, sh), 597 (4.23), 402 (4.23), 302 (4.63), 290 (4.69). UV-Vis (powder, praying mantis DRA), 648(sh), 608, 377, 285. Anal. Cald for $C_{44}H_{34}N_8O_8$: C, 61.49; H, 3.75; N, 13.04. Found: C, 61.47; H, 3.82; N, 12.96

COF-5. A 4 mL screw-cap vial was charged with triphenylene tris(acetonide) **4** (0.020 g, 0.045 mmol) and 1,4-benzenediboronic acid **5** (0.025 g, 0.15 mmol). A 1:1 mixture of mesitylene:dioxane (1:1, 1.0 mL) was added and the gray mixture was sonicated for 15 min. $BF_3{\cdot}OEt_2$ (15 μL, 0.12 mmol) was added, and the mixture was sonicated for another 15 min. The heterogeneous mixture was transferred to a Kimble/Kontes KIMAX-51 borosilicate glass ampoule (5 mL, body length 37 mm, outer diameter 16.75 mm, neck length 51 mm) and frozen in a liquid N_2 bath. The ampoule neck was flame-sealed, reducing its length by 20-30 mm. After warming to rt, the suspension was heated to 90 $^{\circ}$C in a gravity convection oven for 3 d. After cooling, the solids were recovered by vacuum filtration and washed with anhydrous CH_3CN (4 mL). The solids were then suspended in a second portion of anhydrous CH_3CN (3 mL) for 12 h, and again recovered by vacuum filtration to provide **COF-5** as a light gray solid (13 mg, 60%). **COF-5**: IR (powder, ATR) 3390, 1705, 1630, 1523, 1495, 1443, 1396, 1348, 1244, 1163, 1078, 1018, 858, 833, 798, 658. PXRD [2θ (relative intensity)] 3.32 (100), 5.96 (20), 6.96 (9), 9.12 (10), 12.48 (5.6), 26.16 (12). These IR and PXRD data match those published previously.

COF-10. Triphenylene tris(acetonide) **4** (0.020 g, 0.045 mmol) and biphenyl-4,4′-diboronic acid **6** (0.036 g, 0.15 mmol) were subjected to the same procedure as for **COF-5** to yield **COF-10** as a light gray-brown solid (12 mg, 48%). IR (powder, ATR) 3248, 1608, 1495, 1444, 1356, 1246, 1165, 1070, 1014, 860, 818, 733, 654. PXRD [2θ (relative intensity)] 2.80 (100), 4.76 (22), 5.56 (8.5), 7.36 (6.7), 9.56 (2.6), 25.90 (4.2). The FTIR and PXRD data match those published previously.

NiPc-PBBA COF. A 4 mL screw-cap vial was charged with Ni phthalocyanine **7** (20 mg, 0.023 mmol) and 1,4-benzenediboronic acid **5** (19 mg, 0.11 mmol). A mixture of mesitylene and 1,2-dichloroethane (1:3.3, 2.6 mL) was added, and the dark blue mixture was sonicated for 15 min. $BF_3{\cdot}OEt_2$ (15 μL, 0.12 mmol) was added, and the mixture was sonicated another 15 min. The dark heterogeneous mixture was transferred to a Kimble/Kontes trimmed-stem KIMAX-51 borosilicate glass ampoule (5 mL, body length 37 mm, outer diameter 16.75 mm, neck length 51 mm) and frozen in a liquid N_2 bath. The ampoule neck was flame-sealed in air using a propane torch, reducing the total

length by 20-30 mm. Upon warming to rt, the ampoule was heated to 120 °C in a gravity convection oven for 6 days. After cooling to rt, the dark solid was isolated by vacuum filtration and was washed with anhydrous CH_3CN (4 mL). The material was suspended in anhydrous CH_3CN (3 mL) overnight, then recovered by filtration to yield **NiPc-PBBA COF** as a dark indigo-blue solid (12 mg, 58%). **NiPc-PBBA COF:** IR (powder, ATR) 1524, 1472, 1423, 1380, 1334, 1268, 1186, 1084, 1040, 1020, 867, 840, 810, 749, 733, 654. PXRD [2θ (relative intensity)] 3.88 (100), 7.80 (15), 11.72 (3.7), 15.64 (1.2), 26.84 (2.8), 28.04 (1.3). UV-Vis (powder, praying mantis DRA), 667, 377(sh), 290. Anal. Calcd for $(C_{44}H_{16}B_4N_8NiO_8)_n$: C, 59.61; H, 1.82; N, 12.64. Found: C, 50.07; H, 1.93; N, 11.39. It has been noted (see main text ref. 1) that elemental analyses of boronate COFs typically provide reduced carbon values from the formation of non-combustible boron carbide byproducts. We also anticipate similar formation of boron nitride byproducts, lowering the nitrogen value. The presence of boron was confirmed by a characteristic B 1s peak in the XPS spectrum with a binding energy of 192.839 eV and an abundance of 5.13% (calculated: 4.97% excluding hydrogens).

C. MALDI-TOF Mass Spectrometry of COF Precursors

Figure S1. MALDI-TOF MS spectrum of triphenylene tris(acetonide) **4**.

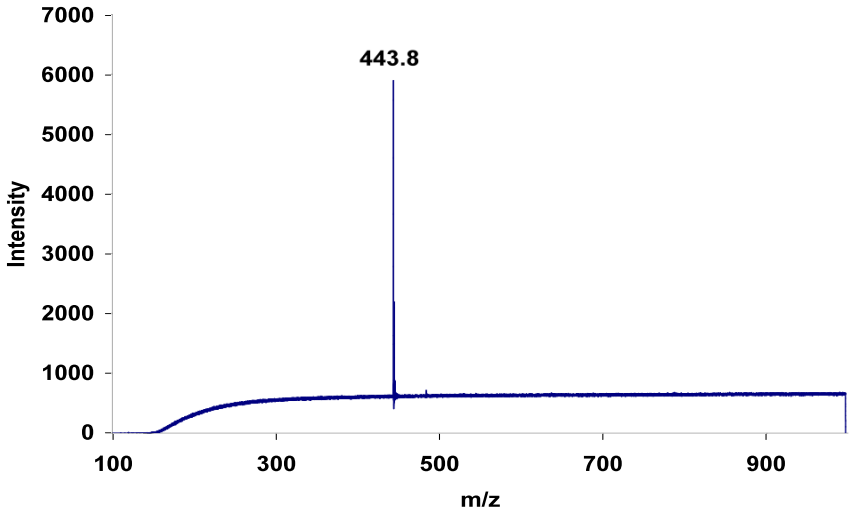

Figure S2. MALDI-TOF MS spectrum of Ni phthalocyanine tetrakis(acetonide) **7**.

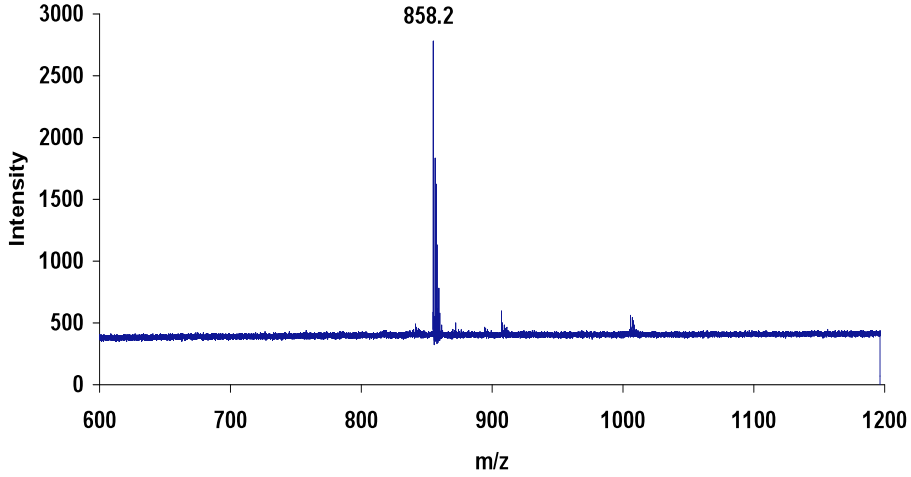

D. Infrared Spectroscopy of COFs and Precursors

Figure S3. Infrared spectra of HHTP tris(acetonide) **4** (top, green), benzene diboronic acid **5** (middle, blue) and **COF-5** (bottom, black).

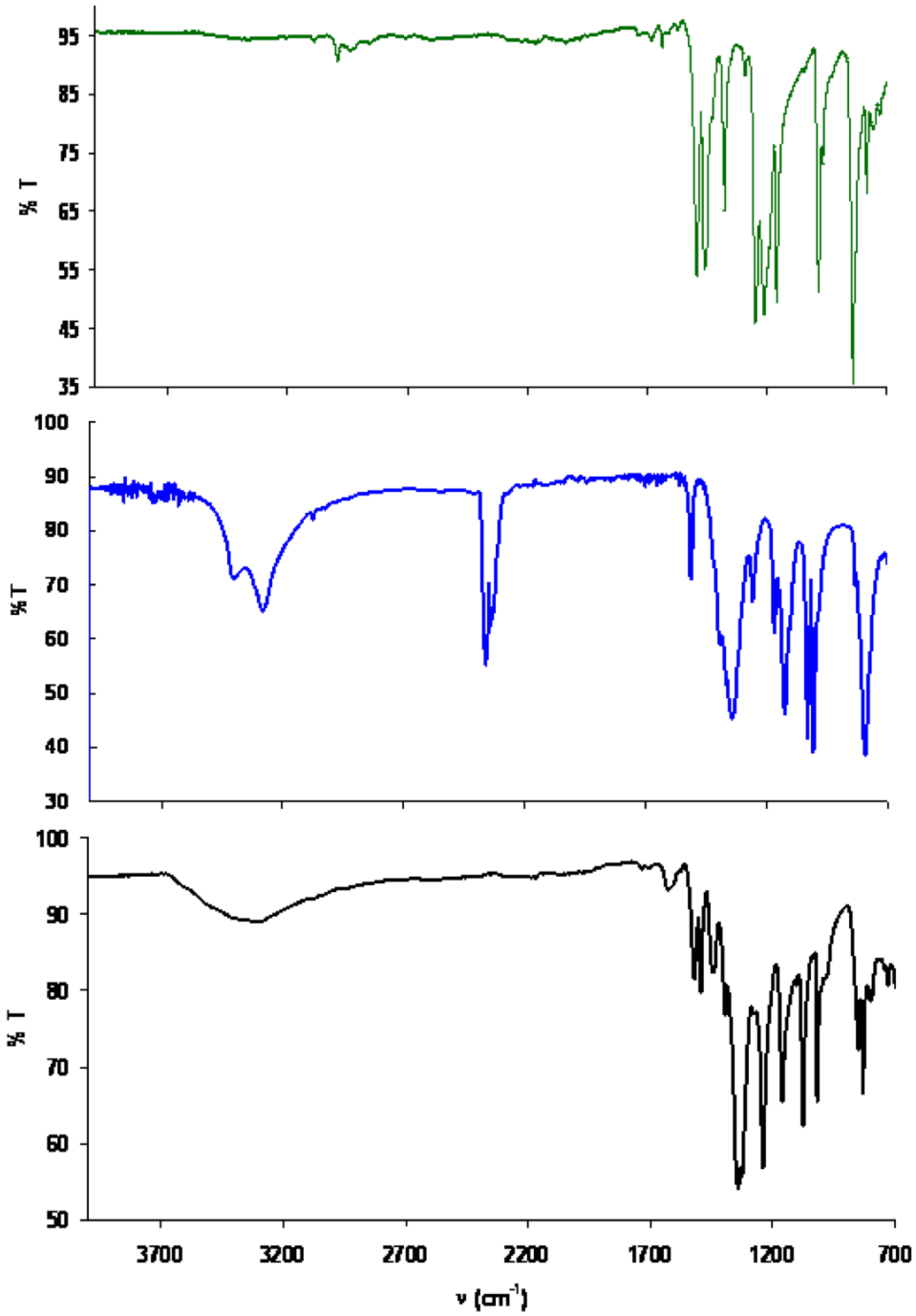

Figure S4. Overlaid infrared spectra of starting materials **4** (green), **5** (blue) and **COF-5** (black) in the 700 to 1700 cm^{-1} region. Note intense 1348 cm^{-1} stretch, characteristic for boronate esters.

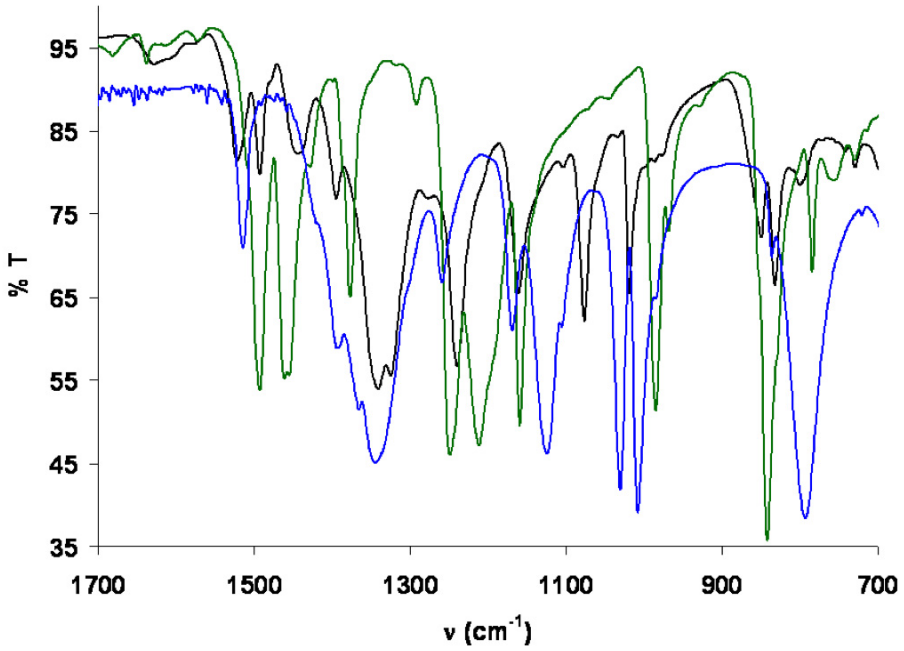

Figure S5. Infrared spectra of biphenyl diboronic acid **6** (top, blue) and **COF-10** (bottom, black).

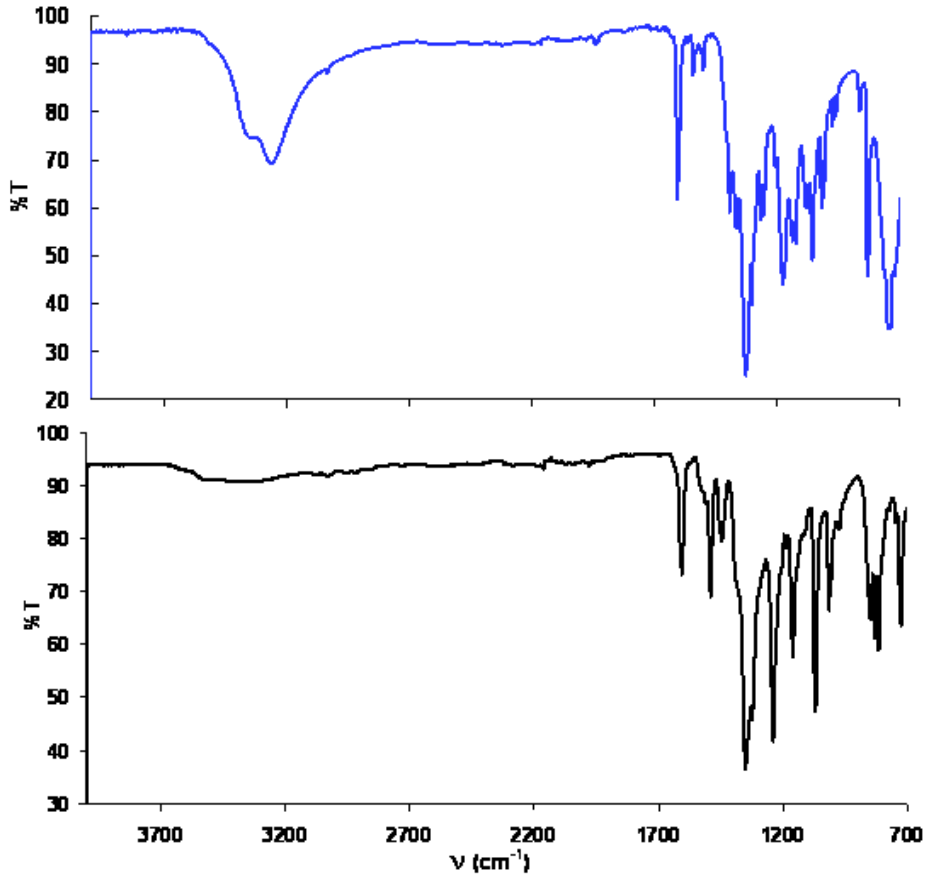

Figure S6. Overlaid infrared spectra of staring materials **4** (green), **6** (blue) and **COF-10** (black) in the 700 to 1700 cm^{-1} region. Note intense 1356 cm^{-1} stretch, characteristic for boronate esters.

.

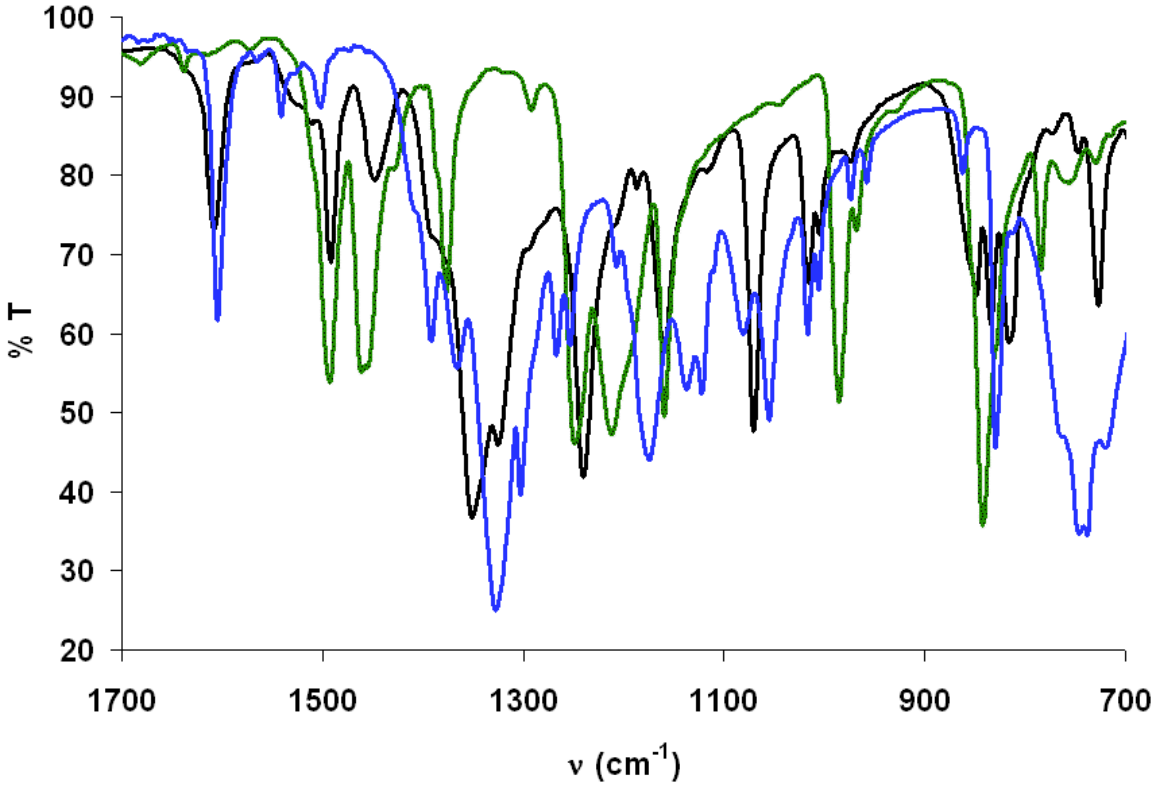

Figure S7. Infrared spectra of Ni phthalocyanine acetonide **7** (top, green), benzene diboronic acid **5** (middle, blue) and **NiPc-PBBA COF** (bottom, black).

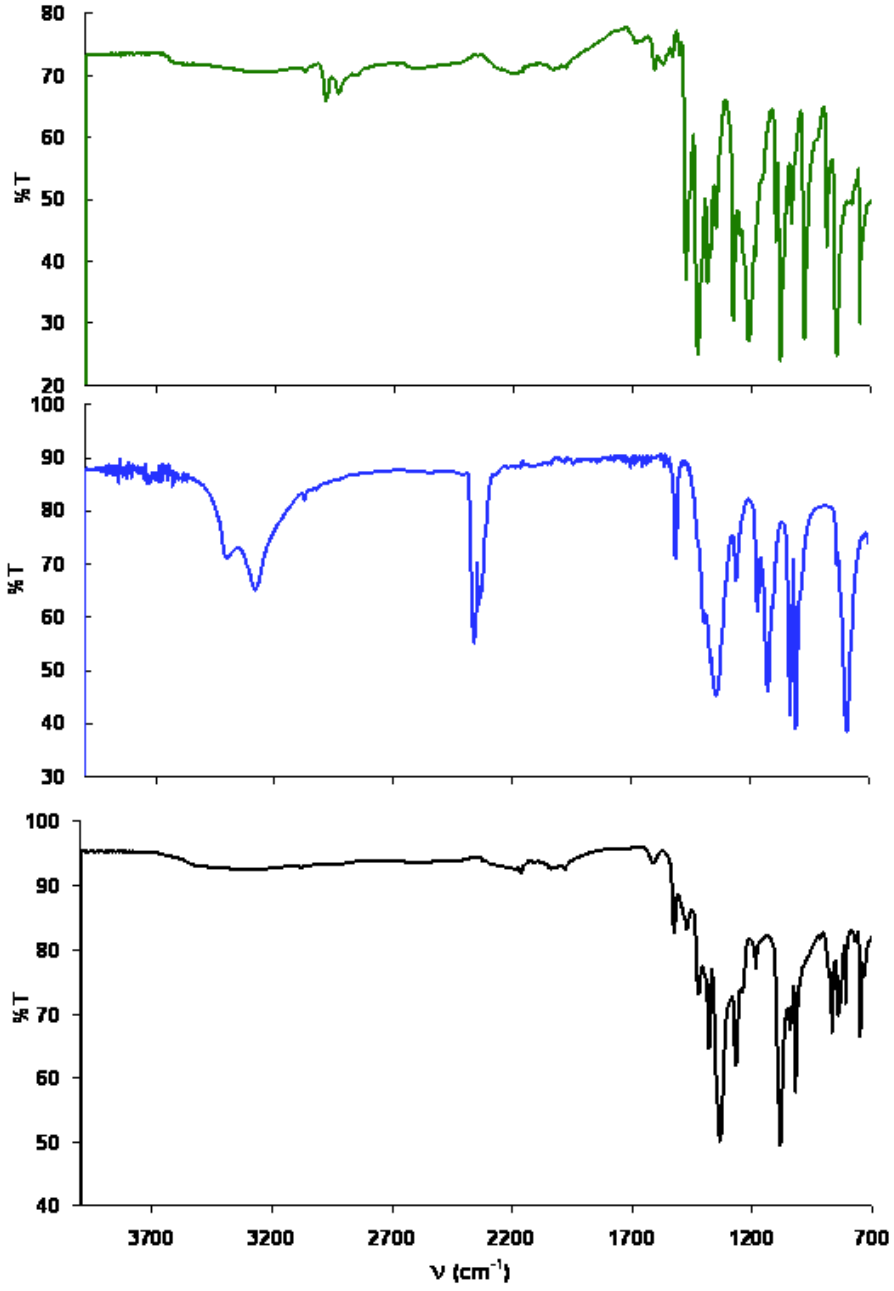

Figure S8. Overlaid infrared spectra of starting materials **5** (blue), **7** (green) and **NiPc-PBBA COF** (black) in the 700 to 1700 cm^{-1} region. Note intense 1334 cm^{-1} stretch, characteristic for boronate esters.

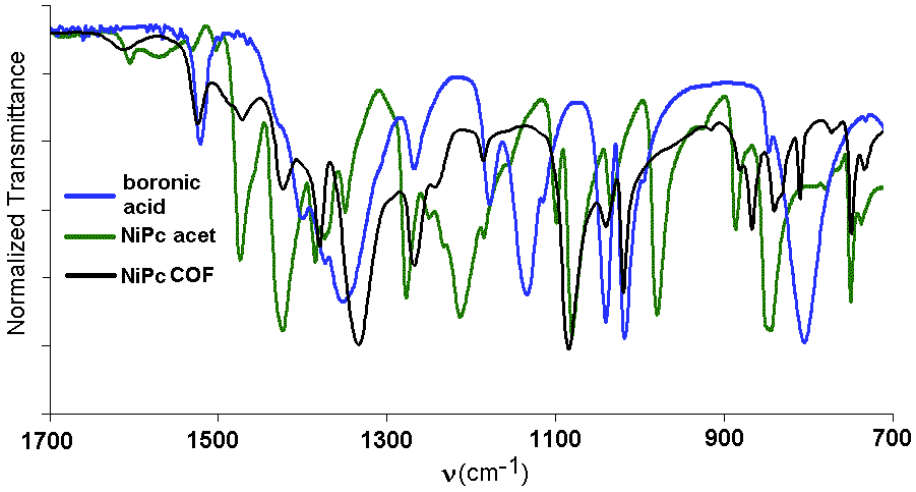

E. COF Surface Area Determination.

Figure S9. BET surface area analysis plots for **COF-5** (blue diamonds), **COF-10** (red squares), and **NiPc-PBBA COF** (green triangles). Q = quantity N_2 adsorbed.

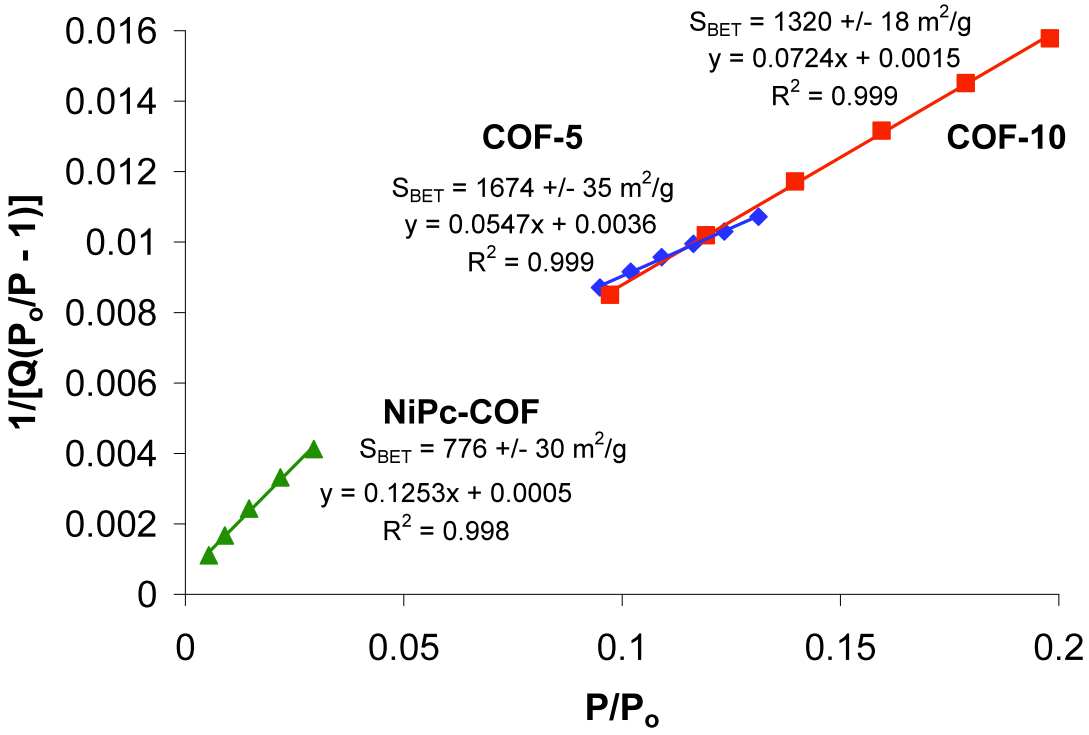

F. Simulation of the NiPc-PBBA COF Structure. Molecular modeling of the COF was carried out using the Materials Studio (ver.4.4) suite of programs by Accelrys[5] in the same manner as our previously-reported free base Pc COF.[4] The unit cell precursor was defined as one phthalocyanine cycle bonded via four boronate ester linkages at the 2,3,9,10,16,17,23, and 24 positions to a benzene ring. The initial structure was geometry optimized using the MS Forcite molecular dynamics module (Universal force fields, Ewald summations), and the resultant distance between opposite benzene ring centroids in the structure was used as the *a* and *b* lattice parameters in a tetragonal D_{4h} crystal (hydrogens omitted for calculation). The interlayer spacing *c* was initially chosen as 3.33 Å and the crystal structure was geometry optimized using Forcite. The MS Reflex Plus module was then used to calculated the expected PXRD pattern, which matched the experimentally observed pattern closely in both peak position and intensity (line broadening from crystallite size was not calculated). The observed diffraction pattern was subjected to Pawley refinement wherein peak profile and line shape parameters were refined using the Pseudo-Voigt peak shape function and asymmetry was corrected using the Berar-Baldinozzi function.[4,5] The refinement was applied to the calculated lattice, producing the refined PXRD profile with lattice parameters $a = b = 22.84$ Å and $c = 3.36$ Å. wR_p and R_p values converged to 6.78% and 5.66%, respectively. Overlay of the observed and refined profiles shows good correlation (Fig. S10). The difference plot indicates the region of greatest deviation to be in the very low angle domain where background interference is greatest.

Table S1. Fractional atomic coordinates for unit cell of **NiPc-PBBA COF** calculated using the Materials Studio ver.4.4 modeling program after Pawley refinement.

3D Tetragonal, D_{4h}
(*P*4/*mmm*)
a = *b* = 22.84 Å, *c* = 3.36 Å

atom	*X*	*y*	*z*
C1	0.44785	0.03036	0.50000
C2	0.50000	0.06042	0.50000
C3	0.53088	0.21731	0.50000
C4	0.43790	0.26901	0.50000
C5	0.47061	0.32024	0.50000
C6	0.44691	0.37752	0.50000
O1	0.44691	0.16189	0.50000
B1	0.50000	0.12750	0.50000
N1	0.50000	0.41343	0.50000
N2	0.39484	0.39484	0.50000
Ni1	0.50000	0.50000	0.50000

G. Powder X-ray Diffraction of COFs.

Figure S10. (a) Observed (blue) and Pawley refined (red) PXRD profiles of COF-5 (left) and COF-10 (right). Profile fitting factors are included in the legend. (b) Observed (black) vs. refined (red) PXRD pattern of **NiPc-PBBA COF** and difference plot (blue, observed-refined).

(a)

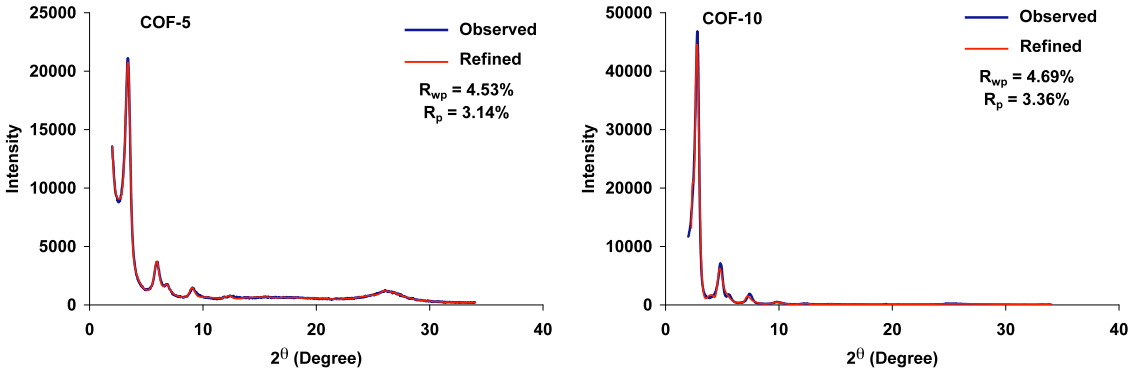

(b)

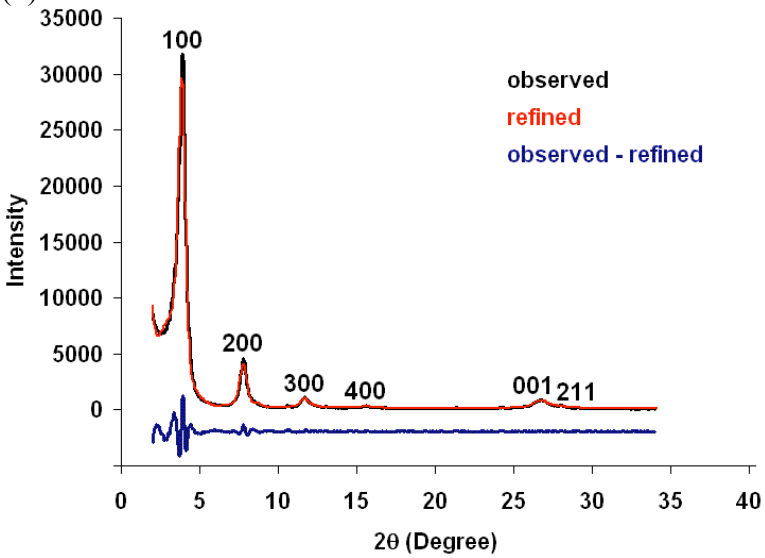

The PXRD pattern is very similar to that observed for the free-base **Pc-PBBA COF** reported previously.[4] The PXRD patterns of the phthalocyanine[4] and boronic acid[6] starting materials show no similarity to the COF pattern.

H. UV/Vis/NIR Spectroscopy of the Ni Pc-PBBA COF and Precursors.

Figure S11. Diffuse reflectance solid state absorption spectra of **7** (blue) and **NiPc-PBBA COF** (red).

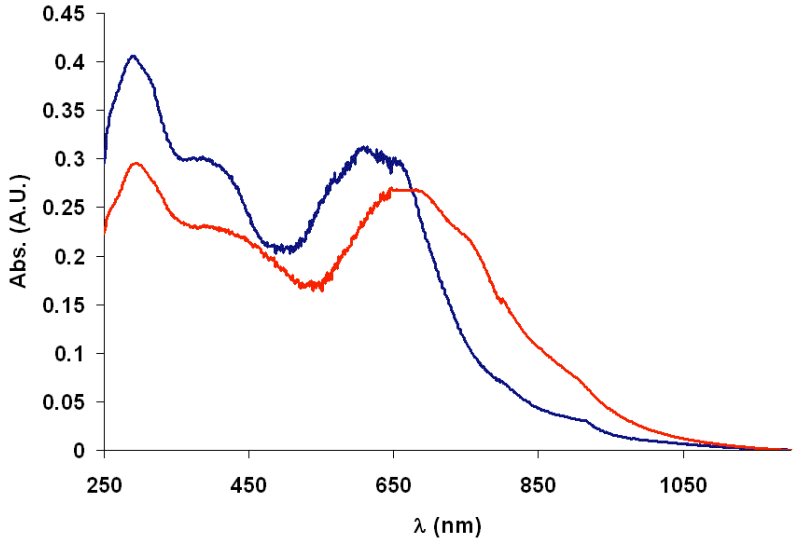

Figure S12. Absorption spectrum of **7** in CH_2Cl_2 solution.

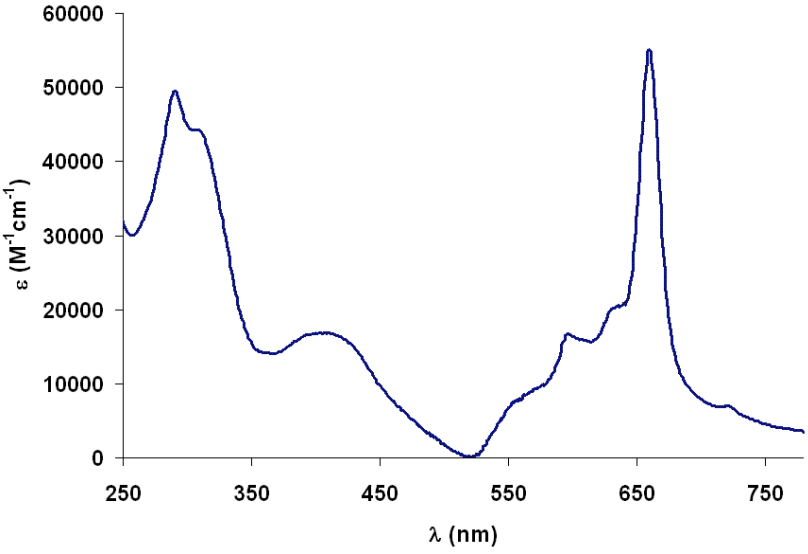

I. Thermogravimetric Analysis of the Ni Pc-PBBA COF.

Figure S13. Thermogravimetric traces of **NiPc-PBBA COF** before (red) and after (blue) 50 ^{o}C overnight preheating under vacuum.

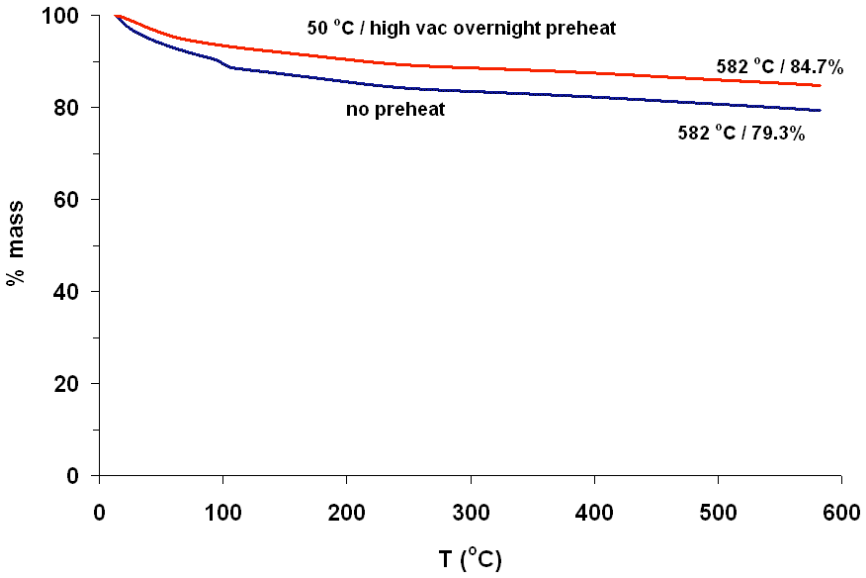

J. Mechanistic Study of Boronate Ester Formation.

Figure S14. Partial ^{1}H NMR spectra ($CDCl_3$, 400 MHz) of the conversion of **1** to **3** under pseudo-first order conditions. $[\mathbf{1}]_0$ = 28 mM; $[\mathbf{2}]_0$ = 560 mM; $[BF_3{\cdot}OEt_2]$ = 14 mM. These data are shown in Figures 3A and plotted in Figure 3C.

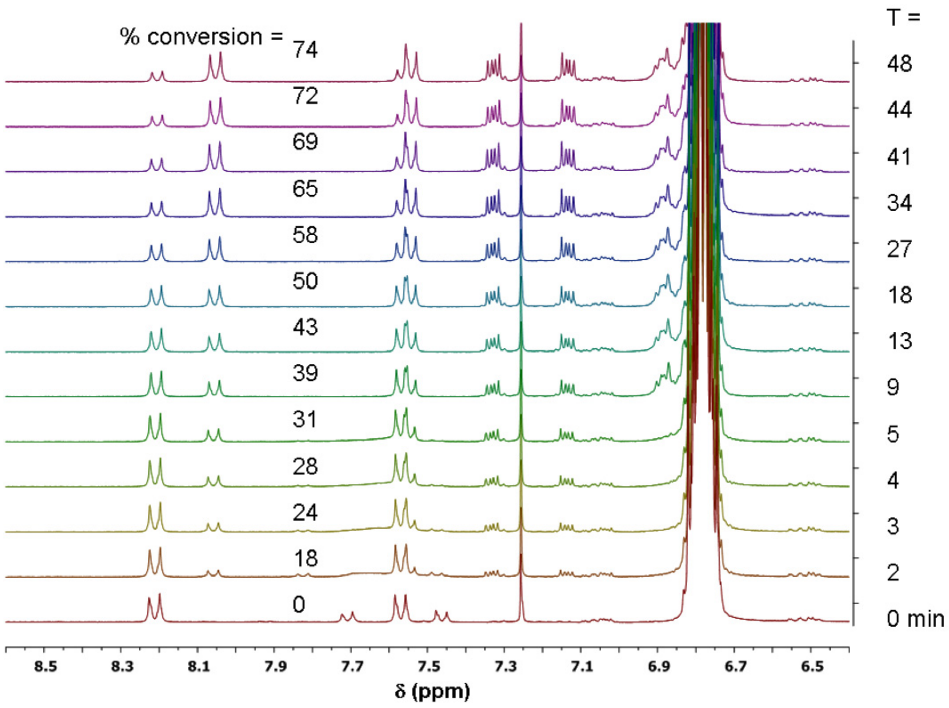

Figure S15. Partial ^{1}H NMR spectra ($CDCl_3$, 400 MHz) of the conversion of **8** to **3** under pseudo-first order conditions. $[\mathbf{8}]_0$ = 9.3 mM; $[\mathbf{2}]_0$ = 560 mM; $[BF_3{\cdot}OEt_2]$ = 14 mM. These data are shown in Figure 3B and plotted in Figure 3C.

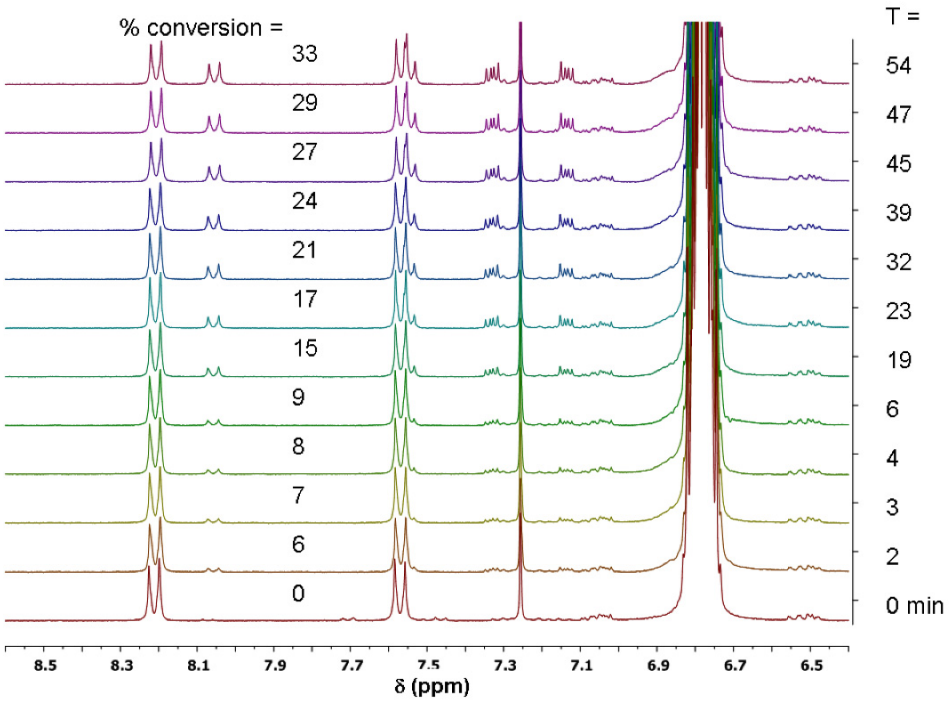

Figure S16. Plot showing the conversion of **1** or **8** to **3** with respect to time under pseudo-first order conditions. The reaction employing **5** as the aryl boronate source (▲) were run under the following conditions: $[\mathbf{1}]_0$ = 28 mM; $[\mathbf{2}]_0$ = 560 mM; $[BF_3{\bullet}OEt_2]$ = 22 mM. The reaction employing **8** as the aryl boronate source (■) was run under the following conditions: $[\mathbf{8}]_0$ = 9.3 mM; $[\mathbf{2}]_0$ = 560 mM; $[BF_3{\bullet}OEt_2]$ = 22 mM. H_2O was added (●) to the reaction employing **8** at t = 10 min.

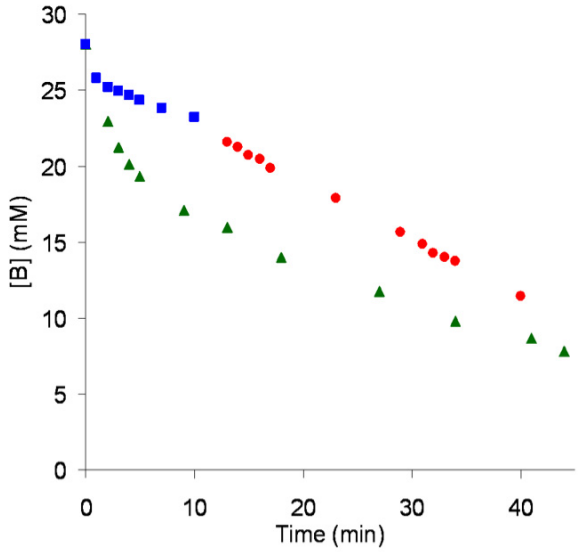

Figure S17. *In situ* infrared spectrum of a CH_2Cl_2 solution of catechol tert-butylphenylboronate **3**. The CH_2Cl_2 background was subtracted. **3** exhibits a distinctive peak at 1335 cm^{-1} that was used in kinetics studies.

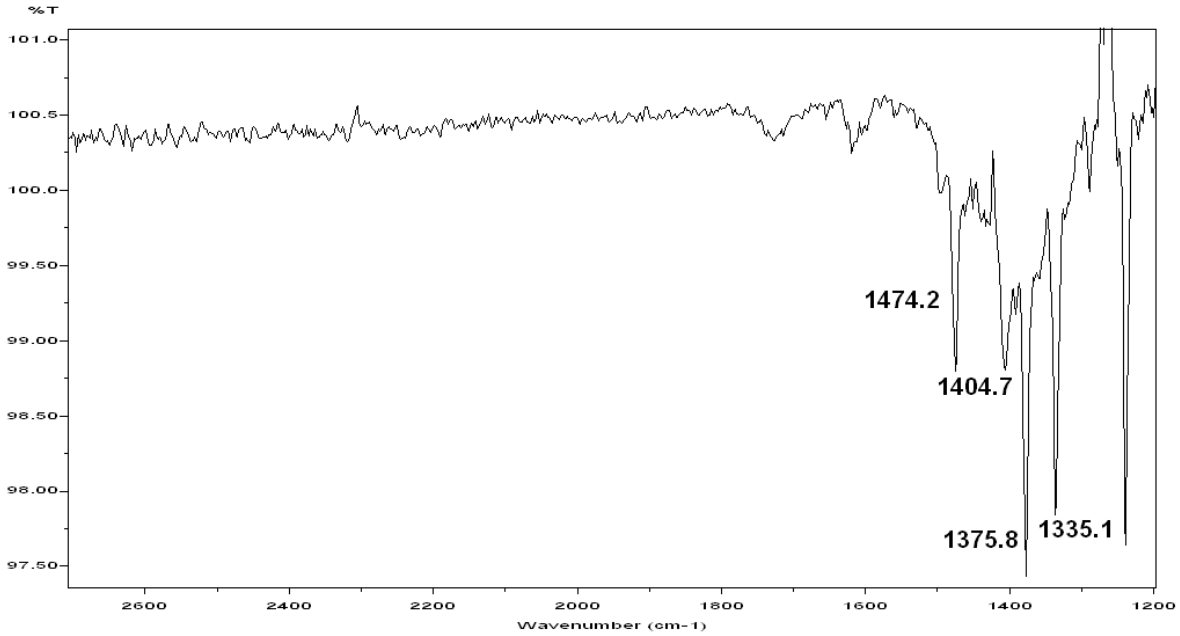

Figure S18. *In situ* infrared spectra of a reaction between catechol acetonide **2** and *t*-butylphenylboronic acid **1** catalyzed by BF_3•OEt_2 over about 3 h. The background of catechol acetonide **2**, BF_3•OEt_2, and CH_2Cl_2 are subtracted.

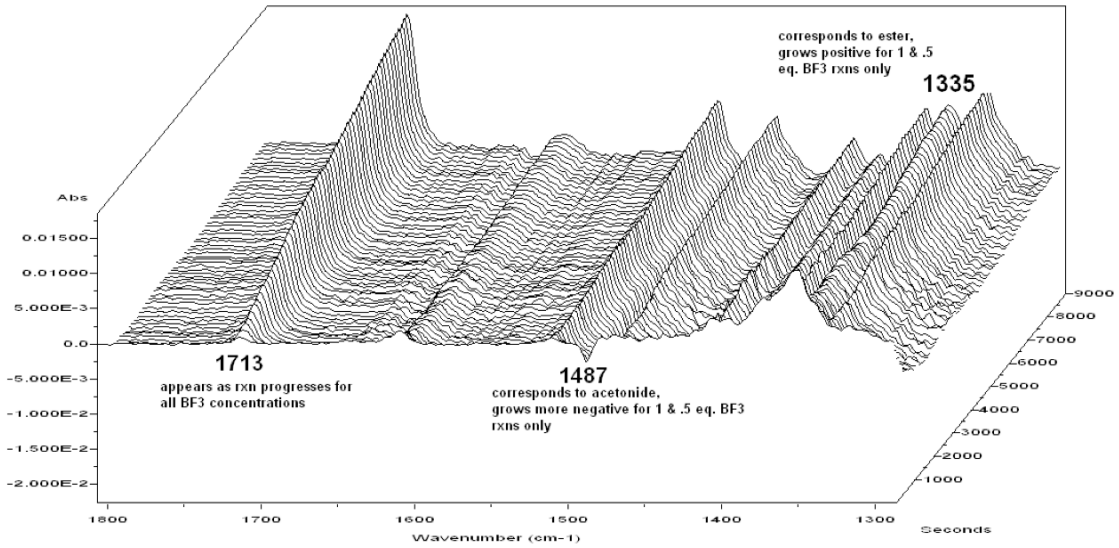

Figure S19. ^{1}H NMR spectra ($CDCl_3$, 400 MHz) of catechol acetonide **2** and varying amounts of BF_3•OEt_2 under anhydrous conditions (red through blue, total time = 1 h) and in the presence of 1 eq. of H_2O (purple). Only minimal acetonide hydrolysis is observed under anhydrous conditions, and the resonances of **2** do not shift significantly in the presence of BF_3•OEt_2. This observation suggests that BF_3 does not strongly bind to **2**. Acetonide hydrolysis does occur in the presence of added H_2O.

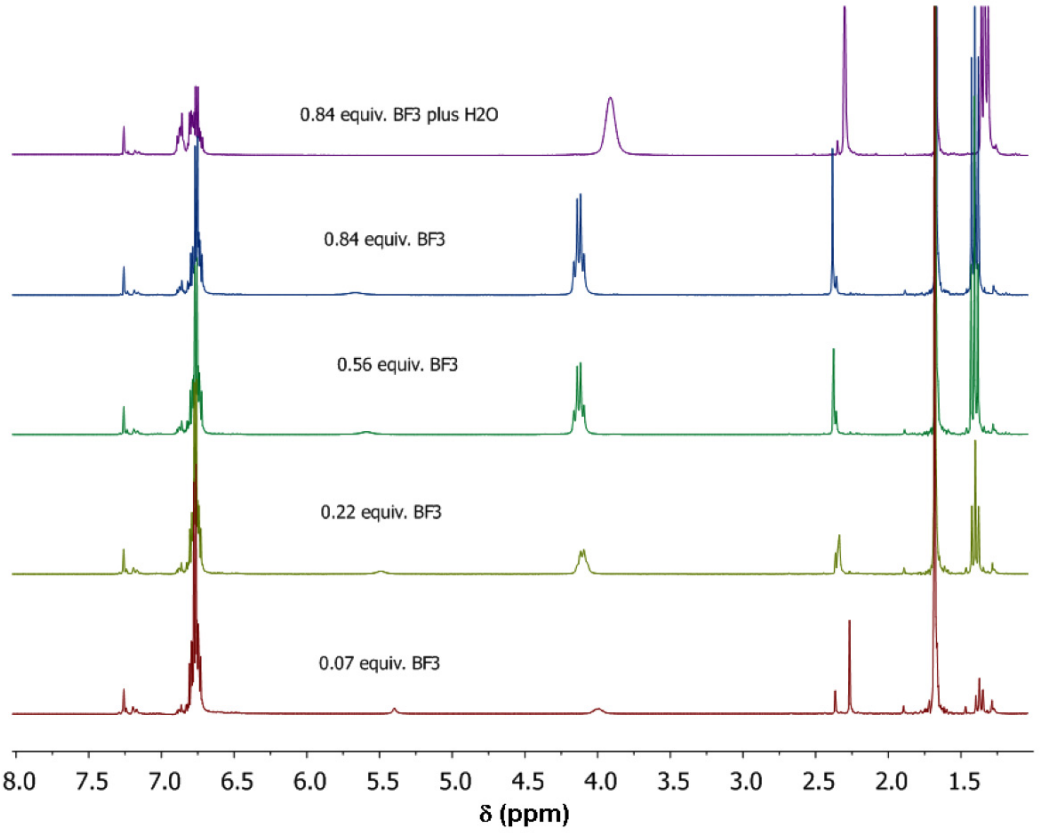

Figure S20. Partial ^{1}H NMR spectra ($CDCl_3$, 400 MHz) of the 2,5-^{1}H resonances of **1** as the [BF_3•OEt_2] is increased. The downfield shift of these resonances is consistent with the formation of the BF_3·**1** complex. Note no observable effect on **8**.

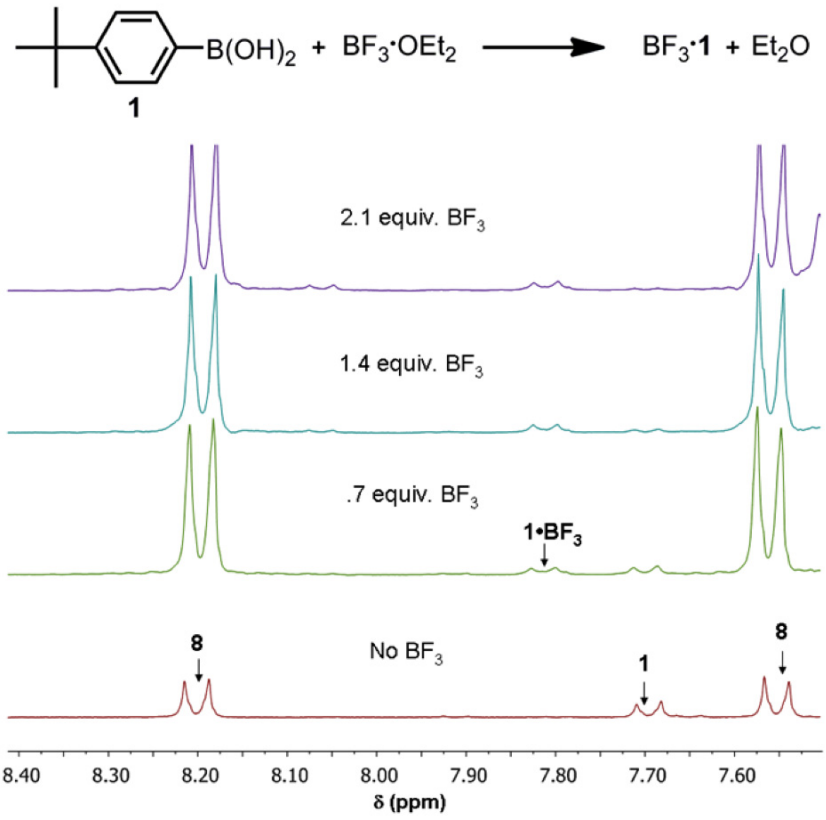

Figure S21. ^{19}F-NMR spectra of increasing BF_3•OEt_2 concentration on 28 mM 4-*t*-butylphenylboronic acid **1** in $CDCl_3$ from 0.1 eq. (bottom) to 1.2 eq. (top) in 0.1 eq. increments. The resonance at -156.5 ppm matches that of BF_3•OEt_2 in $CDCl_3$.

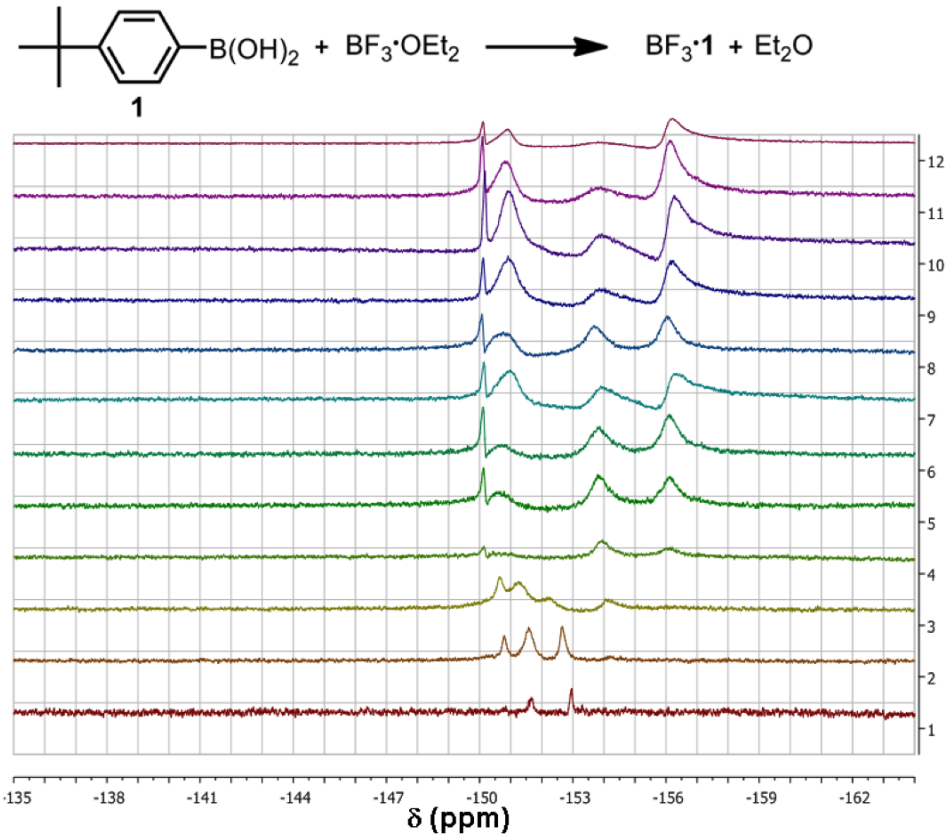

Figure S22. ^{19}F-NMR spectra ($CDCl_3$, 400 MHz) of a reaction mixture containing $[\mathbf{1}]_0$ = 56 mM**,** $[\mathbf{2}]_0$ = 280 mM, and $[BF_3{\bullet}OEt_2]$ = 19 mM. The spectra were taken after 1 h (red), and 22 h (blue-green). Restoration of the $BF_3{\bullet}OEt_2$ resonance at later reaction time occurs as **1** is transformed into **3**.

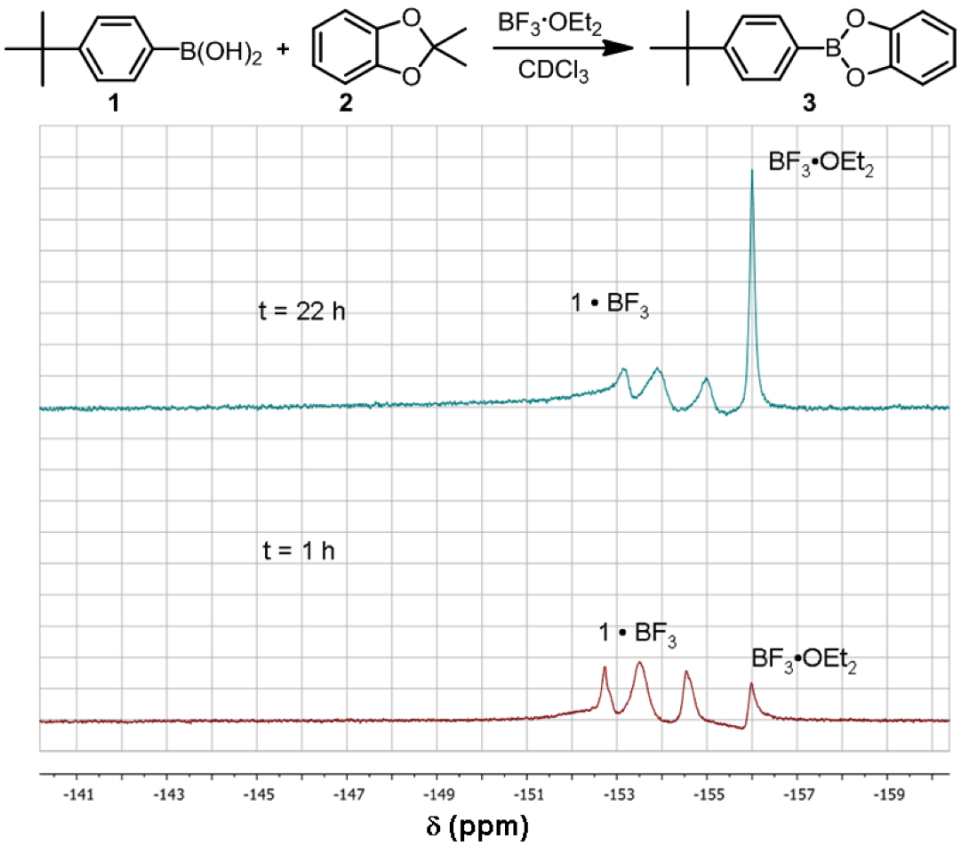

Figure S23. Partial ^{1}H NMR spectra ($CDCl_3$, 400 MHz) of solutions containing equimolar amounts of **1** and catechol. Their condensation to **3** is nearly complete in less than 1 min.

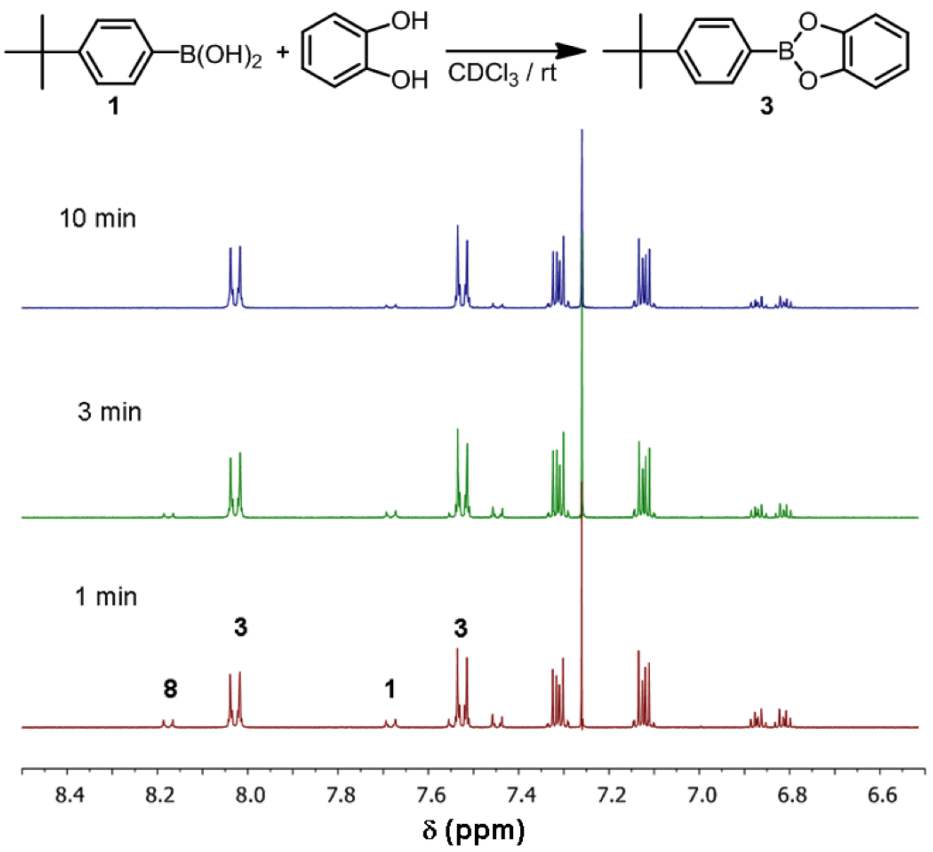

Figure S24. Partial ^{1}H NMR spectra ($CDCl_3$, 400 MHz) of solutions containing **8** and catechol (3 eq.). Their condensation to **3** occurs more slowly than when **1** is employed (see above).

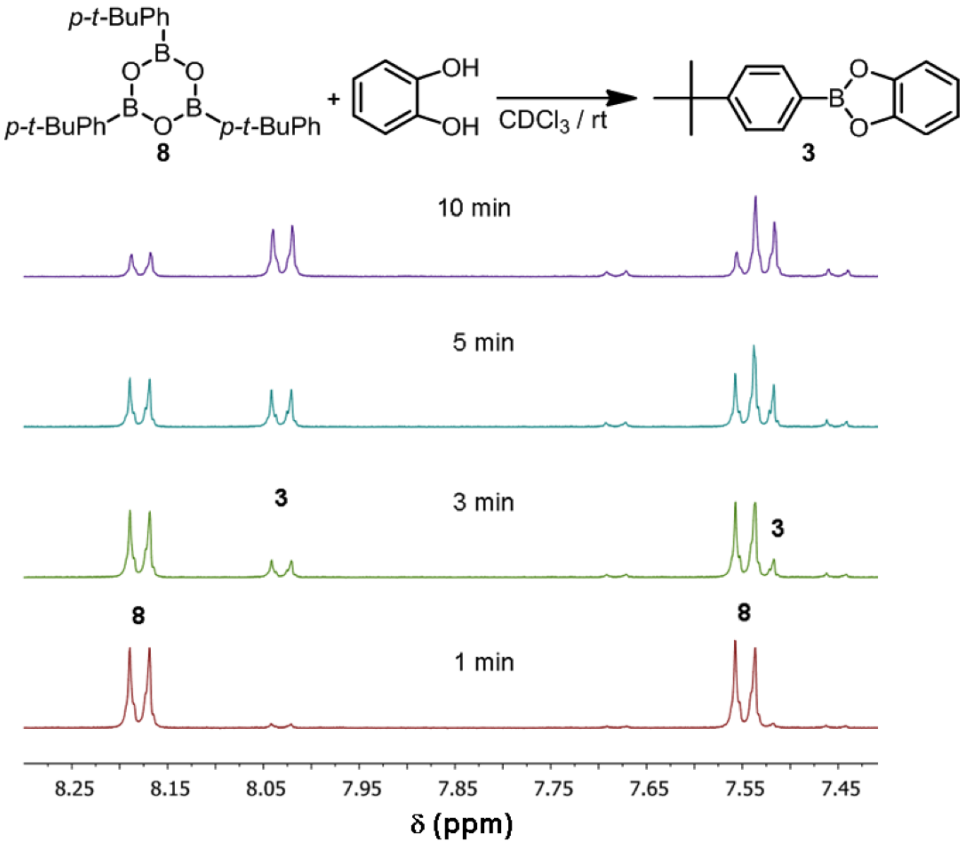

K. Boronate Ester Exchange Experiments.

Catechol *p*-tolylboronate was prepared by refluxing equimolar amounts of catechol and *p*-tolylboronic acid in toluene with azeotropic removal of water followed by evaporation, and 4-methylcatechol phenylboronate was prepared similarly.

The two esters do not exchange in anhydrous $CDCl_3$ (Figure S25), with no changes in their ^1H NMR resonances over 24h. The addition of BF_3•OEt_2 did not play a role in ester exchange. When dissolved in $CDCl_3$ saturated with H_2O, the two boronate esters scramble to a statistical mixture of the four boronate ester products in less than 2 min. None of the respective starting boronic acids or catechols were observed under these conditions.

When equimolar amounts of 4-methylcatechol phenylboronate and catechol are dissolved in anhydrous $CDCl_3$, exchange is also observed without adding additional H_2O (Figure S26). Both esters as well as both catechols are observed. Similarly, when catechol *p*-tolylboronate and phenylboronic acid are combined in a 1:1 ratio in anhydrous $CDCl_3$, acid/ester exchange is also observed (Figure S27). In this case, the exchange is slower, requiring about 30 min for 50% scrambling of products. This is presumably due to the slow hydrolysis of the phenylboronic acid from its initial anhydride form. When 1.5 equivalents of BF_3•OEt_2 is added to the same mixture, more than three hours is required for 50% scrambling (Figure S28). This is most likely because of competitive binding of the BF_3 to the acid, making it unavailable for exchange. These experiments provide strong evidence that the anhydride form of the boronic acid is not the reacting species in the transformation.

Figure S25. ^{1}H-NMR spectra of equimolar (24 mM) mixture of catechol p-tolylboronate **9** and 4-methylcatechol phenylboronate **10** in anhydrous $CDCl_3$ (top, blue), with 160 mM BF_3•OEt_2 added (middle, green), and $CDCl_3$ saturated with H_2O (bottom, red).

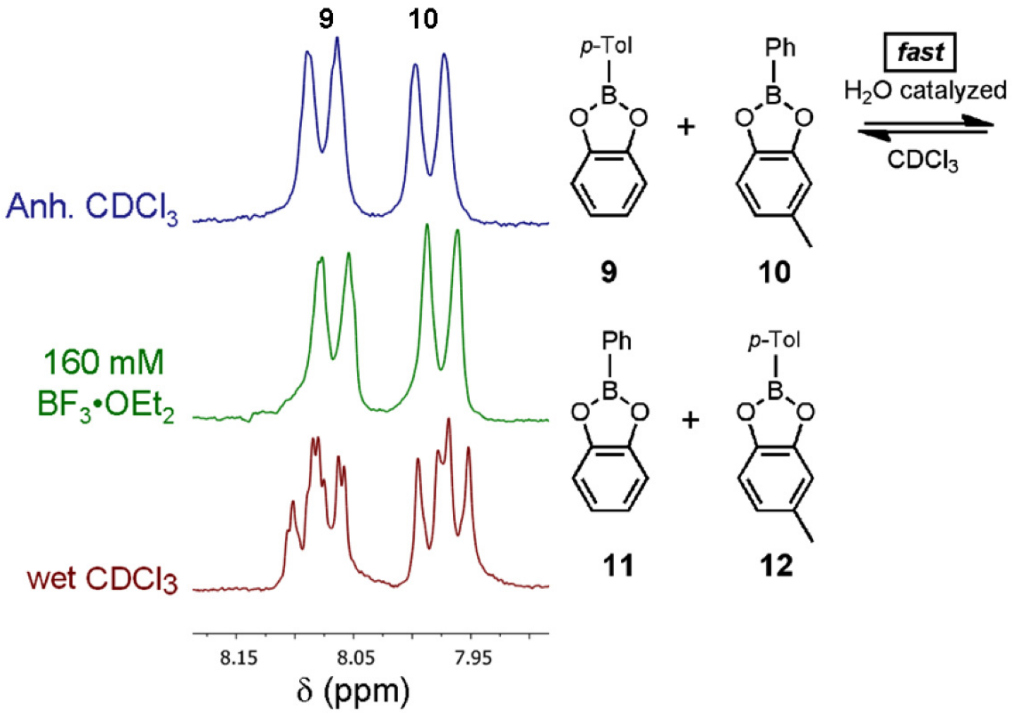

Figure S26. ^{1}H-NMR spectra of 24 mM) 4-methylcatechol phenylboronate **10** in anhydrous $CDCl_3$ (top, blue-green) and with equimolar catechol added (bottom, red).

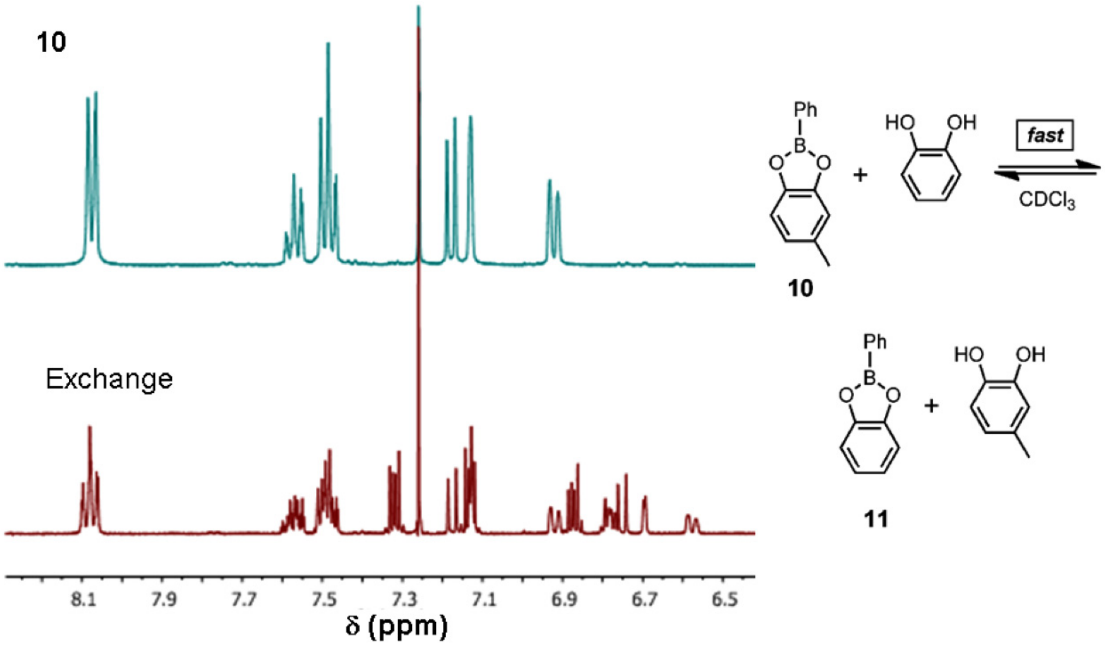

Figure S27. ^{1}H-NMR spectra of equimolar (24 mM) mixture of catechol p-tolylboronate **9** and phenylboronic acid in anhydrous $CDCl_3$ after 1 min(top, blue), 30 min (middle, green), and 60 min (bottom, red).

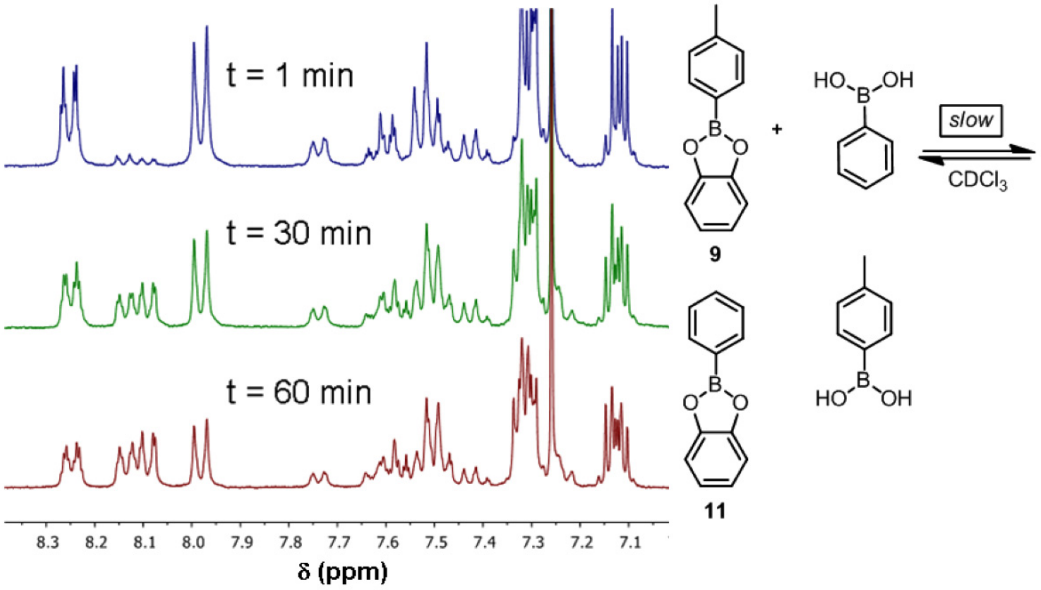

Figure S28. Scrambling between equimolar (24 mM) mixture of catechol *p*-tolylboronate **9** and phenylboronic acid with addition of 1.5 equiv. BF_3•OEt_2.

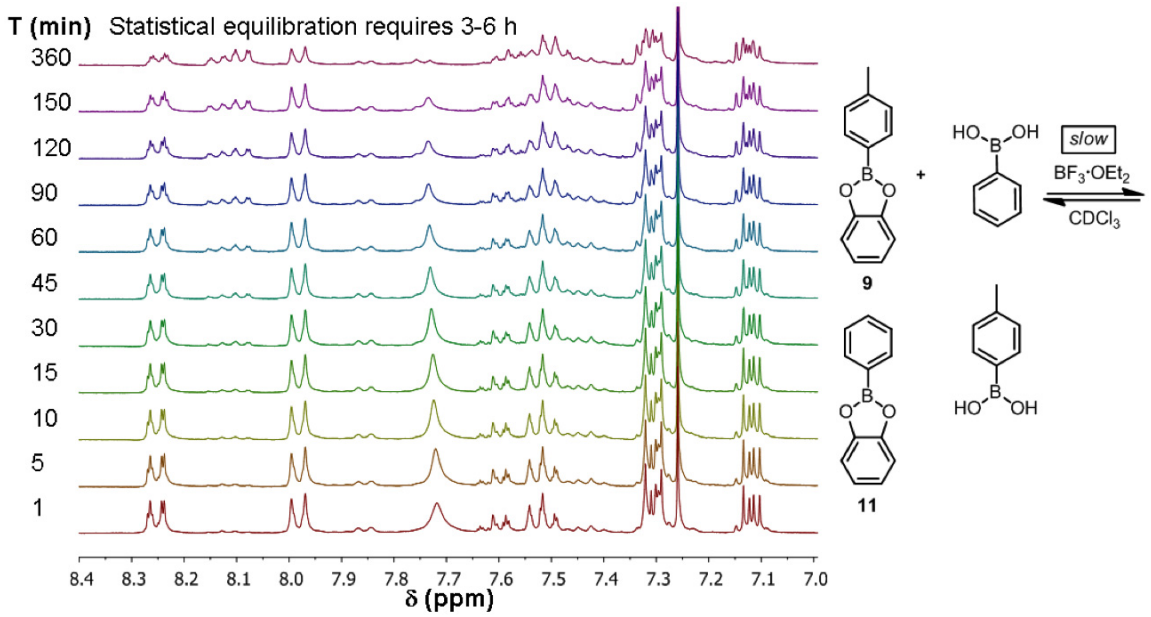

L. References

1. Kumar, S.; Manickam, M. *Chem. Commun*. **1997**, 1615-1616.

2. Waldvogel, S. R.; Mirk, D. *Tetrahedron Lett*. **2000**, *41*, 4769-4772.

3. Rindorf, G.; Bjørnholm, G.; Bechgaard, K. *Acta Cryst*. **1989**, *C45*, 267-269.

4. Spitler, E. L.; Dichtel, W. R. *Nat. Chem*. **2010**, *2*, 672-677.

5. Accelrys, Material Studio Release Notes, Release 4.4, Accelrys Software, San Diego 2008.

6. Campbell, N. L.; Clowes, R.; Ritchie, L. K.; Cooper, A. I. *Chem. Mater*. **2009, *21,*** 204-206.